Electronic and thermoelectric properties of nanograting layers

2014 IOP Conf. Ser.: Mater. Sci. Eng. 60 012025

(http://iopscience.iop.org/1757-899X/60/1/012025)

Electronic and thermoelectric properties of nanograting layers

A Tavkhelidze
Ilia State University, Cholokashvili Ave. 3-5, Tbilisi 0162, Georgia

E-mail: avtotav@gmail.com

Abstract. Recently, new quantum features have been observed and studied in the area of nanostructured layers. Nanograting (NG) on the surface of the thin layer imposes additional boundary conditions on electron wave function and forbids some quantum states. Electrons, rejected from the forbidden quantum states, have to occupy states with higher energy. In the case of semiconductor materials, electrons rejected from the valence band have to occupy empty quantum states in the conduction band. Such increase in conduction band electron concentration n can be termed as geometry-induced doping or G-doping. G-doping is equivalent to donor doping from the point of view of the increase in n. However, there are no ionized impurities. This preserves charge carrier scattering to the intrinsic semiconductor level and increases carrier mobility. G-doping involves electron confinement to NG layer. Here, we investigate the system of multiple NG layers forming a series of homo junctions. Si and GaAs homojunctions were studied and G-doping levels of 10^{18}-10^{19} cm^{-3} were obtained. We also study a system composed of NG layer and an additional top layer forming periodic series of p–n junctions. In such system, charge depletion region develops inside the NG and its effective depth reduces, becoming a rather strong function of temperature T. Consequently, T-dependence of chemical potential magnifies and Seebeck coefficient S increases. We investigate S in the system of semiconductor NG layer having abrupt p–n junctions on the top of the grating. Analysis made on the basis of Boltzmann transport equations shows dramatic increase in S. At the same time, other transport coefficients remain unaffected by the junctions. Calculations show one order of magnitude increase in the thermoelectric figure of merit ZT relative to bulk material.

1. Introduction

Developments in nanotechnology allow fabrication of densely packed, periodic structures [1-4]. Recently, ultra-short period nanopore arrays and nanogratings have been obtained by block copolymer lithography [1, 2]. Another method for nanograting (NG) fabrication is multi-beam interference lithography. Using these techniques, gratings with 10-nm [3] and even sub-10 nm pitch [4] were fabricated. At the same time, it has been shown that NG dramatically improves thermoelectric [5] and electron emission properties [6] when grating pitch becomes comparable with electron de Broglie wavelength. This is owing to special boundary conditions imposed by NG on electron wave function. Supplementary boundary conditions forbid some quantum states, and density of quantum states (DOS) reduces (in all bands). Electrons rejected from NG-forbidden quantum states have to occupy empty states with a higher energy. Fermi energy increases and electronic properties of NG layer change. In the case of semiconductor materials, electrons rejected from the valence band (VB) occupy empty quantum states in the conduction band (CB). Electron concentration n in the CB increases which can

be termed as geometry-induced electron doping or G-doping. G-doping is equivalent to donor doping from the point of view of increase in n and Fermi energy. However, there are no ionized impurities. This maintains charge carrier scattering to intrinsic semiconductor level and increases carrier mobility with respect to the donor-doped layer of same electron concentration. G-doping is temperature independent as it originates from layer geometry and no ionized impurities are involved.

Other methods of doping without impurities are well known modulation doping and recently introduced polarization doping [7]. Both are 2D in their nature. However, a 3D approach of modulation doping was introduced in [8] to improve thermoelelectric characteristics of nanocomposites [9]. Influence of periodic structures on electronic properties has been studied in related geometries such as periodic curved surfaces [10, 11], nanotubes [12], cylindrical surfaces with non-constant diameter [13] and strain-driven nanostructures [14].

Electron confinement to the NG layer is needed to obtain G-doping. The layer can be made free standing but in practice it is usually sandwiched between wide band gap layers. NG layer thickness is fundamentally limited by the requirement of having quantum properties. However, thin layers have low optical absorption. Layer thickness also limits lateral charge and heat transport.

Figure 1 shows a cross section of a single NG layer. The grating has depth a and period $2w$. To make a comparison, we choose reference layer as plain layer with thickness H such that it has the same cross section area.

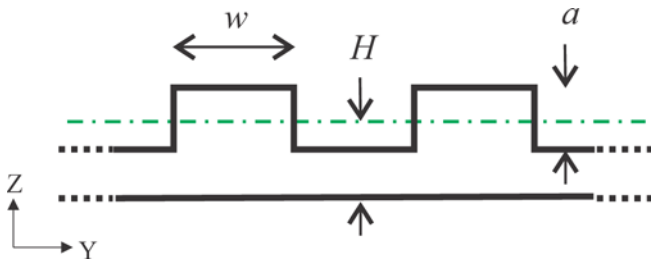

Figure 1. Cross section of nanograting layer.

Nanograting imposes additional boundary conditions on electron wave function and forbids some quantum states. The DOS in energy $\rho(E)$ reduces [15] with respect to the reference well

$$\rho(E) = \rho_0(E)/G \tag{1}$$

Where $\rho_0(E)$ is the DOS (number of quantum states within the unit energy region and in the unit volume) in a reference well and $G = G(H, w, a) > 1$ is the geometry factor. With increasing NG depth a DOS reduces.

Nanograting reduces DOS in all bands. Electrons rejected from the NG-forbidden quantum states have to occupy empty quantum states with higher E. In a semiconductor, electrons rejected from the VB have to occupy empty (and not forbidden by NG) energy levels in CB (figure 2). Electrons reject from low energy levels and occupy high energy ones. During this process, Fermi energy increases from $E_F^{(0)}$ to E_F. To simplify the presentation, in figure 2, we presume that T=0 (T is absolute temperature) and energy levels are equidistant on the energy scale (geometry-induced energy level shift is also ignored).

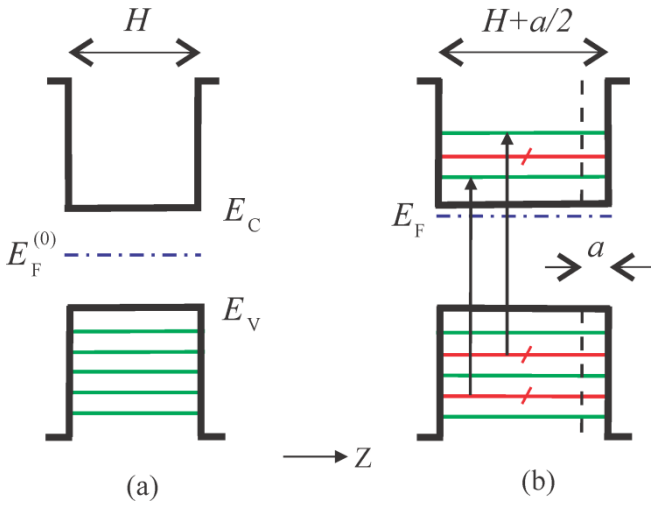

Figure 2. Energy diagrams of a) reference semiconductor quantum well and b) NG layer. Green lines depict occupied energy levels. Red lines depict NG-forbidden energy levels.

We will employ (1) to calculate the DOS and investigate G-dependence of n and E_F. The density of the NG-forbidden quantum states is

$$\rho_F(E) = \rho_0(E) - \rho_0(E)/G = \rho_0(E)(1-1/G). \quad (2)$$

To determine the number of rejected electrons n_r (per unit volume), (2) should be integrated over the electron confinement energy region.

$$n_r = \int_{con} dE\, \rho_F(E) = (1-1/G) \int_{con} dE\, \rho_0(E) = (1-1/G)\, n_{con}. \quad (3)$$

Where, $n_{CON} = \int_{con} dE\, \rho_0(E)$. Here, we assume that electron confinement takes place only in narrow energy intervals inside which G is energy-independent. In most cases, thin layer is grown on a semiconductor substrate and confinement energy regions are band offsets.

To obtain electron confinement in multiple NG layers transitional barrier layers are required. We regard cases of wide band gap material forming heterojunction, and the same material forming homojunction. In heterojunction case, confinement regions are band discontinuities (both type-I and type-II band alignments are considered). In homojunction case, confinement regions originate from barrier layer donor doping.

Here, we investigate G-doping in multiple NG layers. Such layers are quasi-3D and have improved optoelectronic and thermoelectric characteristics with respect to a single layer. Multiple NG layers consist of a replicated structure including main and barrier layers forming a series of hetero or homo junctions. Main layer is thicker than barrier layer and plays a leading role in carrier transport and optical absorption. Barrier layer forms electron confinement energy regions. It also contributes to carrier transport and optical absorption. Both main and barrier layers have NG geometry.

One of the objectives of this work is to calculate n and in multiple NG layers and find out how they depend on layer thicknesses and material properties. First, we introduce G-doping in a single NG layer. Next, we calculate n and in a homojunction multilayer structure. Subsequently, we calculate the same for a heterojunction multilayer structure. Finally, the possibility of realization of such structures and their advantages for optoelectronic and thermo-electric devices are discussed. An analysis was

made within the limits of parabolic band, wide quantum well and degenerate electron gas approximations.

Thermoelectric materials are characterized in terms of dimensionless figure of merit *ZT*. Here, *T* is the temperature and *Z* is given by $Z = \sigma S^2/(\kappa_e + \kappa_l)$, where *S* is the Seebeck coefficient, σ is electrical conductivity, κ_e is electron gas thermal conductivity, and κ_l is lattice thermal conductivity. The difficulty in increasing *ZT* is that materials having high *S* usually have low σ. When σ is increased, it leads to an increase in κ_e, following Wiedemann–Franz law, and *ZT* does not improve much. Another approach is to eliminate the lattice thermal conductivity by introducing vacuum nanogap between the hot and cold electrodes [16–18] and using electron tunnelling. Cooling in such designs was observed in [19] and theoretically studied in [20]. However, vacuum nanogap devices appear extremely difficult to fabricate. In this work, we present a solution that allows large enhancement of S without changes in σ, κ_e, and κ_l. It is based on having series of p–n junctions on the top of the NG.

It is another objective of this work is to calculate *ZT* of NG with series of p–n junctions and compare it with Z_0T of reference nanograting (RNG), in which $G \neq G(T)$, and bulk material. The reduced figure of merit ZT/Z_0T is calculated and μ dependences are presented for such traditional thermoelectric materials as Si and Ge. Analysis was made within the parabolic bands approximation and the abrupt junction's approximation. Since only heavy G-doping was considered, we neglected the hole contribution in transport.

2. Electronic properties of multiple homojunction NG layer

We begin from calculating *n* in a homojunction NG layer, as it is relatively straightforward. Homojunction is formed between intrinsic main layer and donor-doped barrier layer. Let us consider a case when all layers have a plain geometry (NG is not formed yet). Figure 3a shows an energy diagram of such structure (typically obtained by homoepitaxal growth) [21]. Charge depletion regions form inside the both *i*-type main layer and n-type barrier layer. Band edges curve, shaping confinement regions in the main layer VB and in the barrier layer CB. Electrons with energies $E_V - \Delta E_{con}^{(0)} < E < E_V$ are confined to main layers and ones with energies $E_C - \Delta E_{con}^{(0)} < E < E_C$ are confined to barrier layers. Here, we assume that both main and barrier layers are relatively thick so that electron wave functions do not overlap and we can ignore the mini band formation.

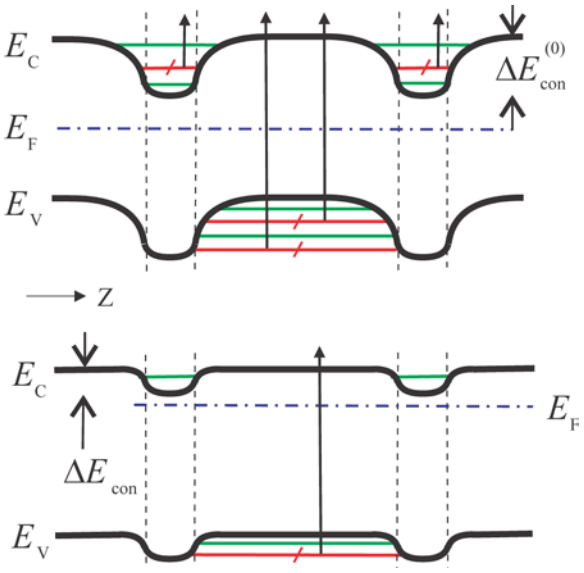

Figure 3. Homojunction structure energy diagrams: a) before NG formation, b) after NG formation. Green lines depict occupied energy levels. Red lines depict NG-forbidden energy levels.

2.1 Influence of Nanograting

Next, we fabricate NG on the surface of all layers simultaneously (fabrication of such structure will be discussed later in this work). NG forbids some energy levels (red lines) and induces G-doping depending on geometry factor value. We introduce two geometry factors G_m and G_b for the main and barrier layers separately (layers have different geometry factors owing to a different thickness).

If $G_m > 1$ some electrons reject from the VB of main layer (figure 3). If $G_b > 1$ some electrons reject from the CB of barrier layer and occupy higher energy levels in the same band. In the beginning, let us regard the case $G_m > 1$ and $G_b = 1$. As $G_m > 1$, the Fermi level increases in main layer, which is equivalent to shifting band edges down on the energy scale. As $G_b = 1$, the bang edges remain intact in barrier layer. With the downward shift in main layer, VB confinement region will shrink and fewer electrons will reject to the CB. This will continue until some equilibrium value of rejected electrons is achieved. In other words, band edge downward shift provides negative feedback to the G-doping process. Next, let us regard the case $G_m > 1$ and $G_b > 1$. Here, barrier layer band edges also shift down. Owing to the downward shift in barrier layer, confinement energy regions widen. This increases the number of rejected electrons in main layer. In other words, barrier layer G-doping provides positive feedback to main layer G-doping. Finally, we have a combination of negative feedback originating from main layer and positive feedback origination from barrier layer. In the case of overall negative feedback G-doping of two layers will saturate and equilibrium value of ΔE_{con} will be attained (figure 3b). Last depends on G_m and G_b and semiconductor material parameters.

2.2 Electron confinement energy region

To find ΔE_{con} we have to calculate electron concentrations in both main and barrier layers first. Applying (2) to the main layer we find the number of rejected electrons

$$n_r = (1 - 1/G_m) \int_{E_V}^{E_V - \Delta E_{con}} dE\, \rho_{0V}(E) \ , \tag{4}$$

where, $\rho_{0V}(E)$ is the initial (to NG) DOS in the main layer VB. Let us regard the case when the rejected electron number is much more than the initial electron number in CB $n_r >> n_0$. Then, the CB electron concentration will be merely n_r. Further, we use the following well known expression for valence band DOS to calculate n_r [22]

$$\rho_{0V}(E) = 2\pi^{-1/2} N_V (k_B T)^{-3/2} (E - E_V)^{1/2} \ . \tag{5}$$

Here, N_V is the effective VB density of states. Inserting (5) in (4) and integrating, choosing zero of energy scale as $E_V = 0$ we find

$$n_r = (4/3\sqrt{\pi}) N_V (1 - 1/G_m)(\Delta E_{con} / k_b T)^{3/2} \ . \tag{6}$$

Further, we find Fermi levels in both layers using corresponding electron concentrations. According to the well known expression for degenerate semiconductor [23] Fermi level in main layer can be found from

$$E_F - E_C^{(m)} = k_B T\left[\ln\left(n_r / N_C\right) + 2^{-3/2}\left(n_r / N_C\right)\right] \tag{7}$$

where, N_C is the effective CB density of states. CB electron concentration of barrier layer does not change during NG formation, as there are no electrons transferred from the VB to the CB. However, Fermi level in the barrier layer moves up on an energy scale owing to NG-induced reduction in N_C

$$E_F - E_C^{(b)} = k_B T\left[\ln\left(G_b\, n_d / N_C\right) + 2^{-3/2}\left(G_b\, n_d / N_C\right)\right]. \tag{8}$$

Here, n_d is barrier layer initial electron concentration (obtained by donor doping). Energy diagram (figure 3) shows that $\Delta E_{con} = E_C^{(m)} - E_C^{(b)}$. Subtracting (7) from (8) and inserting in the last expression we find

$$\left(\Delta E_{con} / k_B T\right) = \ln\left(G_b\, n_d / n_r\right) + 2^{-3/2}\left[\left(G_b\, n_d - n_r\right) / N_C\right]. \tag{9}$$

Inserting (6) in (9) and depicting $\eta \equiv \Delta E_{con} / k_B T$ we get following nonlinear equation for η

$$\eta + \frac{3}{2}\ln\eta + 2^{-3/2}\frac{4}{3\sqrt{\pi}}\frac{N_V}{N_C}\frac{G_m - 1}{G_m}\eta^{3/2} - \ln\frac{3\sqrt{\pi}G_m G_b\, n_d}{4N_V\left(G_m - 1\right)} - 2^{-3/2}\frac{G_b\, n_d}{N_C} = 0\ . \tag{10}$$

Equation (10) was solved numerically to find ΔE_{con} using two geometry factor and n_d, N_C, N_V values for Si and GaAs materials.

2.3 Electron concentration and Fermi level

Numerical solutions of (10) were inserted in (6) to find n_r. Next, we found the Fermi level of the main layer by inserting values of n_r in (7). Formula (8) was used to find a Fermi level position in barrier layer. Table 1 shows the results for geometry factors G_m =1. 02, G_b = 1.1 and *T*=300 K.

Table 1. Electron concentration and Fermi levels in main and barrier layers for Si and GaAs materials. Energy was measured from corresponding layer CB edge.

Material	n_d **[cm^{-3}]**	ΔE_{con} **[meV]**	n_r **[cm^{-3}]**	$E_F^{(m)}$ **[meV]**	$E_F^{(b)}$ **[meV]**
Si	3 x 10^{18}	45	6 x 10^{17}	103	58
	1 x 10^{19}	64	1 x 10^{18}	89	25
	3 x 10^{19}	87	1 x 10^{18}	77	-10
	1 x 10^{20}	126	2.8 x 10^{18}	62	-64
GaAs	1 x 10^{18}	47	3.2 x 10^{17}	3.4	-44
	3 x 10^{18}	86	8 x 10^{17}	-29	-115
	5 x 10^{18}	119	1.3 x 10^{18}	-52	-172
	1 x 10^{19}	197	2.8 x 10^{18}	-110	-297

For barrier donor doping levels 10^{18}-10^{20} cm^{-3} and *G* values rather close to unity (G_m =1.02, $G_b = 1.1$) main layer G-doping levels of 10^{17}-10^{18} cm^{-3} were obtained. We chose this range of G-dropping levels, as they are frequently used in applications. Higher and lower G-doping levels can be obtained as well. Table 1 shows that one order higher donor doping n_d (10^{20} cm^{-3}) is needed in Si with respect to GaAs (10^{19} cm^{-3}) to obtain a G-doping level 2.8 10^{18} cm^{-3}. It is convenient to give an interpretation of this result using terms of negative and positive feedback. Negative feedback in main layer is weaker for Si material as it has higher n_0 value with respect to GaAs. Owing to high n_0, band edges shift down less rapidly with increasing n_r, following well known logarithmic dependence $\Delta E_F = k_B T \ln(n_r / n_0)$. As ΔE_F is positive in our case, higher n_0 results in weaker negative feedback. Weaker negative feedback in the main layer requires weaker positive feedback in the barrier layer to obtain equilibrium. Positive feedback is weaker in highly donor-doped barrier layers (as shifting band edges require more rejected electrons). This explains why higher n_d is required in Si barrier layer with respect to GaAs.

As figure 3 shows there are potential barriers for electrons in the CB and holes in the VB of multilayer NG. They are affecting carrier transport in Z direction. However, barrier height is ΔE_{con} which is of the order of a few $k_B T$ as table 1 indicates (except for very high level of donor doping. $k_B T$ =26 meV for *T*=300 K). Charge carriers easily overcome such obstacles (thermionic emission) and their influence can be ignored. In the case of high values of ΔE_{con} barriers may block carrier transport in Z direction. To avoid this, high level of G-doping should be obtained not by increasing donor doping of barrier layers but by increasing of G_m and G_b values.

During numerical calculations, we kept $E_F^{(m)}$ and $E_F^{(b)}$ in proximity of corresponding CB edges to stay within the limits of degenerate electron gas approximation (so that (7) and (8) are valid). For lower doping levels, other expressions should be used instead of (7) and (8).

2.4 G-doping for high electron mobility applications

Realization of G-doping is attractive from the point of view of high mobility applications. Let us use a multi junction solar cell [24] as an example to estimate G-doping improvement of its characteristics. In this device, window, emitter and tunnel junction layer doping levels are roughly 10^{18} cm^{-3}. At this level of donor doping, ionized impurities reduce electron mobility by a factor of 4 in GaAs [25] (at *T*=300 K) and by the factor of 10 in Si [26]. Most types of solar cells use transparent conductive oxides with doping levels of 10^{20}-10^{21} cm^{-3}. At this donor doping level ionized impurities reduce electron mobility by the factor of 30-50 in GaAs. Thus, using G-doping in these layers can dramatically improve characteristics of solar cells.

Multiple NG layers can be realized by epitaxial growth on the top of lead grating, previously formed on the substrate. Such structure has been modelled [27] and fabricated [28] on GaAs substrate using epitaxial growth technique. Layers, grown using this technique, have diverse geometry compared to single NG layer. They have gratings from both sides and interfaces resemble sine instead of square. With increasing number of layers sine amplitude reduces and finally one gets plain layers. Geometry factor and G-doping level reduce with increasing of layer number.

It is challenging to obtain high *G* values or considerable DOS reduction in both NG and alike geometries. However, as table 1 show, G-doping required values are quite close to unity (especially for the main layer). The obtaining of such values in multiple NG systems seems to be straightforward.

The above analysis was made using the assumption of *G* energy independence (3). Usually, electron confinement energy regions are small (tens or hundreds of meV) and this assumption is valid. However, the NG layer can be made free standing or grown on very wide band gap substrate. In these

cases, confinement energy intervals are much wider and care should be taken when assuming *G* energy independence.

3. Charge and heat transport in the NG layer with p-n junctions

Here, we propose a system composed of NG layer and an additional layer on the top of the ridges forming periodic series of p^+–n^+ junctions (figure 4). In such system, charge depletion region develops

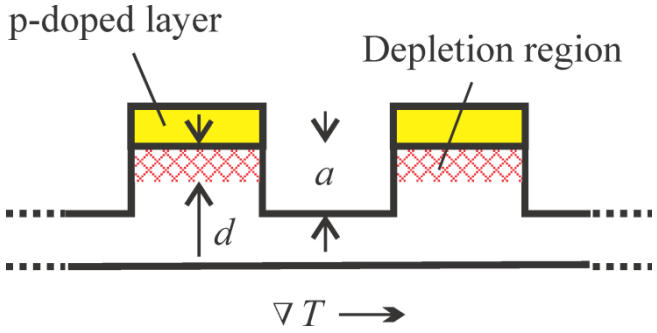

Figure 4. NG with series of periodic junctions grown at the top of the ridges.

inside the ridges and effective ridge height reduces, becoming a rather strong function of temperature *T*. Consequently, *T*-dependence of chemical potential μ magnifies and Seebeck coefficient *S* increases. Depletion region width $\mathrm{d}(T)$ depends rather strongly on temperature. The ridge effective height $a_{\mathrm{eff}}(T) = a - \mathrm{d}(T)$ and consequently the geometry factor *G* becomes temperature-dependent, $\mathrm{G} = \mathrm{G}(T)$. All parameters of NG layer including μ become stronger functions of *T* than it will be in an NG layer layer without the junctions. Seebeck coefficient and thermoelectric figure of merit increase.

Analysis was made using the Boltzmann transport equations. First, we calculate $\nabla\mu$ for the system of NG layer and junctions and express it as

$$\nabla\mu = \nabla\mu_0 + \nabla\mu_{\mathrm{J}}. \tag{11}$$

Here, $\nabla\mu_0$ is the chemical potential gradient in an RNG (NG layer without p-n junctions) and $\nabla\mu_{\mathrm{J}}$ is introduced by the junctions. Next, we insert $\nabla\mu$ in Boltzmann transport equations and calculate *S* for the system of NG layer and junctions, expressing it as $S = S_0 + S_{\mathrm{J}}$, where S_0 is Seebeck coefficient of RNG and S_{J} is introduced by the junctions..

Cross-section of the system of NG and periodic junction is shown in figure 4. We assume that there is a temperature gradient ∇T in the Y-dimension. Consequently, depletion depth depends on the Y-coordinate, and geometry factor gradient ∇G appears in the Y-direction. Presence of ∇G and ∇T modifies the electron distribution function and causes electron motion from the hot side to the cold side. This motion is compensated by thermoelectric voltage. Let us write Boltzmann transport equations [29] for the system of RQW and periodic series of junctions

$$J = \mathbf{L}^{11}\left(\mathcal{E} + \nabla\mu/e\right) - \mathbf{L}^{12}\nabla T \quad \text{and} \quad J^Q = \mathbf{L}^{21}\left(\mathcal{E} + \nabla\mu/e\right) - \mathbf{L}^{22}\nabla T. \tag{12}$$

Here, J is the electric current density, J^Q is the heat current density, $\mathbf{L}^{ij}$ are coefficients, $\mathcal{E}$ is the electric field, and e is the electron charge. Within the parabolic bands approximation, $\mathbf{L}^{ij}$ are the functions of integrals of type [30].

$$\Omega^{(\alpha)}(E) = \int_{-\infty}^{+\infty} dE\left(-\partial f_0/\partial E\right)\rho(E)\tau(E)\mathrm{v_y}^2(E-\mu)^{\alpha} \tag{13}$$

where f_0 is the electron distribution function, $\tau(E)$ is the electron lifetime, $\mathrm{v_y}$ is the electron velocity in the Y-direction, and α = 0, 1, 2. Let us find how NG affects $\Omega^{(\alpha)}(E)$. The NG does not change dispersion relation and consequently $\mathrm{v_y}$. It reduces density of states (3D density) G times, i.e. $\rho(E) = \rho_0(E)/G$ and increases the transport lifetime G times [31], i.e., $\tau(E) = G\tau_0(E)$ (the latter follows from Fermi's golden rule). Here, $\rho_0(E)$ and $\tau_0(E)$ are the density of states and carrier lifetime, respectively, in the case a = 0. Consequently, product $\rho(E)\tau(E)\mathrm{v_y}^2$ in the NG layer is the same as in the conventional wide quantum well of the same width (3D case) and in the bulk material. This product does not depend on G and consequently it becomes independent of depletion depth. The NG changes the distribution function f_0, since it increases μ. The NG influences integrals $\Omega^{(\alpha)}(E)$ by changing μ alone. Therefore, integrals are the same as in the bulk material having the corresponding chemical potential

$$\mathbf{L}^{ij} = \mathbf{L}_0^{ij}. \tag{14}$$

where $\mathbf{L}_0^{ij}$ are the coefficients of bulk material having the value of μ obtained by the conventional doping (for instance).

Further, we have to find μ for the system of NG layer and junctions and insert it in (12) together with (14). Chemical potential of degenerated semiconductor ($-2 < \mu^* < 2$ where $\mu^* = \mu/k_BT$) can be written as [32] (note that frequently Fermi energy is used instead of chemical potential in semiconductor literature)

$$\mu = k_BT\left[\ln\left(n/N_{NG}\right) + 2^{-3/2}\left(n/N_{NG}\right)\right]. \tag{15}$$

where n is the electron concentration and N_{NG} is the effective conduction band density of states of NG layer. In the case of heavy G-doping ($n >> n_i$, where n_i is intrinsic concentration), we can use (3) for n. Density of states reduces G times in NG layer, i.e. $N_{NG} = N_C/G$, where N_C is the CB effective density of states for bulk semiconductor. Inserting this and (3) in (15), we get

$$\mu = k_BT\left\langle\ln\left[n_{con}(G-1)/N_C\right] + 2^{-3/2}\left[n_{con}(G-1)/N_C\right]\right\rangle. \tag{16}$$

Further, we rewrite (16) as

$$\mu = \mu_0 + k_BT\left\langle\ln\left[(G-1)/(G_0-1)\right] + 2^{-3/2}\left(G-G_0\right)n_{con}/N_C\right\rangle \tag{17}$$

where G_0 is constant. Introduction of $\mu_0 \equiv \mu(G_0)$ defines reference material as n$^+$-type semiconductor with electron concentration of $N_D = n_{CON}(G-1)$, or RRQW having constant geometry factor $(\partial G/\partial T) = 0$ and $G = G_0$. Next, we calculate the gradient of (10) taking into account that $N_C \propto T^{3/2}$. The result is

$$\nabla\mu = \nabla\mu_0 + \theta\nabla T \ . \tag{18}$$

$$\text{where } \theta \equiv k_B\left[\ln\frac{G-1}{G_0-1} - \frac{1}{2}\xi\left(G-G_0\right) + T\left(\frac{1}{G-1}+\xi\right)\frac{\partial G}{\partial T}\right] \tag{19}$$

and $\xi \equiv 2^{-3/2} n_{con}/N_C$. Inserting (18) and (14) in Boltzmann equations, we find charge and heat currents in the system of NG layer + Junctions

$$J = \mathbf{L}_0^{11}\left(\mathcal{E} + \nabla\mu_0/e\right) - \left(\mathbf{L}_0^{12} - \mathbf{L}_0^{11}\theta/e\right)\nabla T \ \text{ and} \tag{20a}$$

$$J^Q = \mathbf{L}_0^{21}\left(\mathcal{E} + \nabla\mu_0/e\right) - \left(\mathbf{L}_0^{22} - \mathbf{L}_0^{21}\theta/e\right)\nabla T \ . \tag{20b}$$

Further, Seebeck coefficient, electrical conductivity, and electron gas heat conductivity can be found from (20a) and (20b) in a conventional way.

$$S = \left(\mathbf{L}_0^{12} - \mathbf{L}_0^{11}\theta/e\right) \Big/ \mathbf{L}_0^{11} = S_0 - \left(\theta/e\right), \tag{21}$$

$$\kappa_e = \mathbf{L}_0^{22} - \mathbf{L}_0^{21}(\theta/e) - \left(\mathbf{L}_0^{12} - \mathbf{L}_0^{11}\theta/e\right)\mathbf{L}_0^{21}\Big/\mathbf{L}_0^{11} = \kappa_{e0}, \tag{22}$$

$$\sigma = \mathbf{L}_0^{11} = \sigma_0. \tag{23}$$

Electrical and thermal conductivity in the system of NG layer and junctions remain unaffected (with respect to RNG layer or bulk material having the same μ value) by a series of junctions, and *S* change according to (21). To calculate θ and then *S*, we have to find $\partial G/\partial T$ first (19).

Such performance of transport coefficients has following physical interpretation. The geometry factor G is a rather strong function of temperature. Consequently, *T*-dependence of chemical potential magnifies and Seebeck coefficient, having approximate value $S \approx -(1/e)(\partial\mu/\partial T)$, increases. Electrical conductivity $\sigma = \Omega^{(0)}$ is G independent since, the reduction of state density leads to proportional increase of lifetime, according to Fermi's golden rule (resulting in (14)). In a degenerate electron gas (n^+-type semiconductor) Wiedemann–Franz law works well. Thus, the thermal conductivity κ_e follows σ and is also G independent.

4. Seebeck coefficient of NG layer with p–n junctions

It is reasonable to calculate Seebeck coefficient of NG layer with junctions relative to RNG layer, in which geometry factor is constant $(\partial G/\partial T) = 0$. This will allow comparison of dimensionless figure of merit *ZT* with Z_0T, using similarity of electric (23) and heat conductivities (22). In (17)–(19) G_0 is

arbitrary. To simplify the comparison, we choose G_0 so that NG layer with junctions and reference RNG layer have the same μ value. Equation of chemical potentials leads to $G_0 = G$ (16). Inserting this in (19) and further inserting the obtained result in (21), we obtain for Seebeck coefficient of NG layer with junctions

$$S = S_0 - \frac{k_B T}{e}\left(\frac{1}{G-1} + \xi\right)\left(\frac{\partial G}{\partial T}\right) . \tag{24}$$

3D Seebeck coefficient of reference RNL do not differ from Seebeck coefficient of the bulk material, and within the parabolic bands approximation it is equal to [33]

$$S_0 = \frac{k_B}{e}\left[\frac{r+5/2}{r+3/2}\frac{\mathrm{F}_{r+3/2}(\mu^*)}{\mathrm{F}_{r+1/2}(\mu^*)} - \mu^*\right] . \tag{25}$$

Here, r refers to scattering parameter and it is assumed that electron lifetime $\tau(E) \propto E^r$, $\mu^* = \mu / k_B T$ is the reduced chemical potential, and $\mathrm{F}(\mu^*)$ are Fermi integrals. In the case of no impurities (G-doping) and low energies, acoustic phonons are responsible for electron scattering and $r = 0$. It should be noted here that NG layer has G times more width [31] with respect to the conventional layer. As 3D $\rho(E)$ in wide quantum wells tends to $\rho(E)$ of the bulk material of the same width, using (28) for RNG is a good approximation. However, in the case of thin layers oscillatory behaviour of transport coefficients should be considered [34].

To find the ratio Z / Z_0, we use relations (22) and (23) and obvious relation between lattice thermal conductivities $\kappa_l = \kappa_{l0}$, all together leading to

$$Z / Z_0 = \left(S / S_0\right)^2 . \tag{26}$$

Figure 5 shows the dependence $S_0(\mu)$ according to (25). The $S(\mu)$ in the same figure is determined by first, calculating $S(G)$ by inserting $\partial G / \partial T$ (which was calculated in [5]) in (24), and then (16) was used to convert X-axis so that $S(\mu)$ was obtained from $S(G)$. The ratio $Z(\mu) / Z_0(\mu)$ in the same figure is calculated according to (26). We present μ dependences as they allow the understanding of possible μ ranges, within which real devices can operate without changing sign of $(\partial G / \partial T)$ (see reference 5) and consequently S sign.

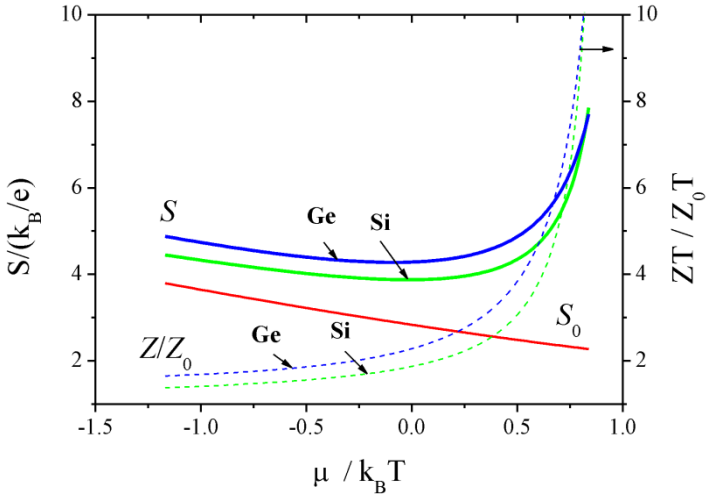

Figure 5. $S(\mu)$ – solid lines, $S_0(\mu)$ – dotted line, and $Z(\mu)/Z_0(\mu)$ – dashed lines (belong to right Y-axis). Dependences $S(\mu)$ and $Z(\mu)/Z_0(\mu)$ are calculated for Si and Ge materials.

Traditional thermoelectric materials Si and Ge are chosen as examples. Dependences are plotted for the following parameters: Material Si, n_{CON} = 4.5×10^{18} cm^{-3}, a = 20 nm, $\gamma = 3.3$ (γ is reduced chemical potential of p-type layer), $\beta = 0.1$ ($\beta = a_{eff}/d$), T = 300 K; Material Ge, n_{con} = 1.4×10^{18} cm^{-3}, a = 35 nm, $\gamma = -1$, $\beta = 0.25$, T = 300 K. For both Si and Ge, we choose n_{con} so that, for value G=10, μ was close to the optimum value $\mu_{OPT}/k_BT = r + 1/2$ [33]. It should be noted here that NG layer exhibits quantum properties at G times more widths with respect to the conventional quantum well.

Figure 5 shows large enhancement of figure of merit in p+–n+ junction NG layer both for Si and Ge materials. The dependences are quite identical for materials having rather different band gaps (1.12 eV for Si and 0.66 eV for Ge). This shows that despite band gap value entering expressions for depletion depth (Reference 5) and $(\partial G/\partial T)$, almost similar $S(\mu)$ and $Z(\mu)/Z_0(\mu)$ dependences can be obtained by matching such parameters as β and γ.

5. Conclusions

Geometry-induced electron doping (G-doping) was investigated in multiple NG layers. They were composed of main and barrier layers forming a series of isotype homo junctions. Barrier layers were used to form electron confinement energy regions. Both main and barrier layers were n-type. Barrier layers were donor-doped to obtain electron confinement and induce G-doping in main layers. Such parameters as electron concentration, Fermi level and confinement region width were calculated for this system. Main layer G-doping level of 10^{17} -10^{18} cm^{-3} was obtained at barrier layer donor doping of 10^{18} -10^{20} cm^{-3} and geometry factor values G_m=1.02, $G_b = 1.1$. One order higher donor doping was required in Si with respect to GaAs to obtain the same G-doping level. For high electron mobility it was preferable to have high values of geometry factors. Electron mobility was higher in G-doped layers with respect to donor-doped layers of same doping level. G-doping opens prospects for new quasi-3D optoelectronic and thermoelectric systems. At the same time G-doping is temperature independent and can be used to extend working temperature ranges of cryogenic and power electronics.

Thermoelectric transport coefficients were investigated in the system of NG layers and periodic series of p–n junctions at the top of the ridges. Analysis was made on the basis of Boltzmann transport

equations. It was shown that the Seebeck coefficient increases considerably. At the same time, electrical and thermal conductivities remain unaffected by the series of junctions. This allows large enhancement of thermoelectric figure of merit. Dependence of Seebeck coefficient on geometry factor G and junction parameters was investigated and the analytical expression was obtained. Seebeck coefficient changes sign for some value of *G*. Dependences of *S* and *ZT* on chemical potential were presented for p–n junction NG layers. Calculations show one order of magnitude increase in thermoelectric figure of merit with respect to the bulk material.

6. Acknowledgements

Author thanks Ismat S. Shah and Juejun Hu for useful discussions. Apparatus received from EU TEMPUS project 530278-TEMPUS-1-2012-1-DE-TEMPUS-JPHES was used for preparing this work for publication.

7. References

[1] Andreozzi A, Lamagna L, Seguini G, Fanciulli M, Schamm-Chardon S, Castro C and M Perego M 2011 Nanotechnology 22 335303

[2] Xia G, Jeong S-J,Kim J E, Kimand B H, Koo C-M and Kim S O 2009 Nanotechnology 20 225301

[3] Paivanranta B, Langner A, Kirk E, David C and Ekinci Y 2011 Nanotechnology 22 375302

[4] Bergmann K, Danylyuk S V and Juschkin L 2009 J. Appl. Phys. 106 073309

[5] Tavkhelidze A 2009 Nanotechnology 20 405401

[6] Tavkhelidze A, 2010 J. Appl. Phys. 108 044313

[7] Simon J, Protasenko V, Lian C, Xing H and Jena D 2010 Science 327 60-64

[8] Yu B, Zebarjadi M, Wang H, Lukas K, Wang H, Wang D, Opeil C, Dresselhaus M,Chen G, and Ren Z 2012 Nano Lett. 12 20772082

[9] H. J. Goldsmid 2010 Introduction to Thermoelectricity (Springer)

[10] Ono S, Shima H 2010 Physica E 42 1224-1227

[11] Kartashov Y V, Szameit A, Keil R, Vysloukh V A, and Torner L 2011 Optics Letters 36 3470

[12] Gupta S and Saxena A 2011 J. Appl. Phys. 109 074316

[13] Fujita N 2004 J. Phys. Soc. Jpn. 73 3115-3120

[14] Ortix C, S. Kiravittaya S, Schmidt O G, and van den Brink J 2011 Phys. Rev. B. 84 045438

[15] Tavkhelidze A and Svanidze V 2008 Int. J. Nanosci. 7 333

[16] Despesse G and Jager T 2004 J. Appl. Phys. 96 5026

[17] Wachutka G and Gerstenmaier Y C 2006 proc. Int. Conference on Mixed Design (MIXDES Poland) p 48

[18] Goldsmid, H J 2003 in Thermoelectrics, 2003 Twenty-Second International Conference on ICT pp 433- 438

[19] Hishinuma Y, Geballe T H, and Moyzhes B Y 2003 J. Appl. Phys. 94 4690

[20] Zeng T 2006 Appl. Phys. Lett. 88 153104

[21] A. Sanders et al 2011 Nanotechnology 22 465703

[22] Sze S M and Ng K K 2007 Physics of Semiconductor Devices (New Jersey: Wiley-Interscience)

[23] Joyce W B and Dixon R W 1977 Appl. Phys. Lett. 31 354

[24] Kirk A P 2010 Solar Energy Materials & Solar Cells, 94 2442

[25] Casey H C Jr, Panish M B 1978 Hetrostructure lasers (Academic, New York)

[26] Bulucea C 1993 Solid-State Electron. 36 489

[27] Ohtsuka M and Suzuki A 1993 J. Appl. Phys. 73 7358

[28] Pickrell G W, Xu C F, Louderback D A, Lin H C, Fish M A, Hindi J J, Simpson M C, Guilfoyle P S, Zhang Z H and Hsieh K C 2004 J. Appl. Phys. 96 4050

[29] Ashkroft N E and Martin N D 1976 Solid State Physics (Saunders College Publishing, NY)

[30] Mahan J D and Sofo J O, 1996 Proc. Natl. Acad. Sci. USA 93 7436

[31] Tavkhelidze A, Svanidze V 2008 Int. J. of Nanoscience 7 333

[32] Joyce W B and Dixon R W 1977 Appl. Phys. Lett. 31 354

[33] Bhandari C M, Rowe D M 1995 CRC Handbook of Thermoelectrics, ed Rowe D M (CRC Press), p 43

[34] Rogacheva E I, Nashchekina O N, Grigorov S N, Us M A, Dresselhaus M D and Cronin S B 2002 Nanotechnology 13 1